Heterogeneous Reactions of Carbonyl Sulfide on Mineral Oxides: Mechanism and Kinetics Study

Yongchun Liu, Jinzhu Ma, Hong He

State Key Laboratory of Environmental Chemistry and Ecotoxicology, Research Center for Eco-Environmental Sciences, Chinese Academy of Sciences, Beijing, 100085, China

Correspondence to: Hong He (honghe@rcees.ac.cn)

Abstract. The heterogeneous reactions of carbonyl sulfide (OCS) on the typical mineral oxides in the mineral dust particles were investigated using a Knudsen cell flow reactor and an *in situ* diffuse reflectance UV-vis spectroscopy. The reaction pathway for OCS on mineral dust was identified based on the gaseous products and surface species. The hydrolysis of OCS, and succeeding oxidation of intermediate products, readily take place on α-Al_2O_3, MgO, and CaO. The reversible and irreversible adsorption of OCS on α-Fe_2O_3 and ZnO were observed, respectively. No apparent uptake of OCS by SiO_2 and TiO_2 was observed. The reactivity of OCS on these oxides is determined by basicity of oxides and the decomposition ability of oxides for H_2S. The uptake coefficient (γ_{BET}) of mineral dust was estimated to be from 3.84×10^{-7} to 2.86×10^{-8} based on the individual uptake coefficients and chemical composition of authentic mineral dust. The global flux of OCS due to heterogeneous reactions and adsorption on mineral dust was estimated at 0.13-0.29 $Tg\cdot yr^{-1}$, which is comparable to the annual flux of OCS for its reaction with ·OH.

1. Introduction

Carbonyl sulfide (OCS) is the predominant sulfur containing compound in the atmosphere, with a rather uniform mixing ratio of about 500 pptv in the troposphere (Chin and Davis, 1995). About 0.64 $Tg \cdot yr^{-1}$ of OCS in the troposphere is transported to the stratosphere, where it can be photodissociated as well as oxidized via reactions with $O(^3P)$ atoms and OH radicals to form sulfate aerosols. Therefore, it has been considered to be a major source of the stratospheric sulfate aerosol (SSA) during volcanic quiescent periods (Andreae and Crutzen, 1997; Crutzen, 1976; Notholt, 2003; Turco et al., 1980). Because the SSA plays an important role in the Earth's radiation balance, global climate (Anderson, et al., 2003; Graf, 2004; Jones et al., 1994), and stratospheric ozone depletion (Andreae and Crutzen, 1997; Solomon et al., 1993), the investigation about the sources and sinks of OCS in the troposphere is very significant in atmospheric chemistry.

In the past decades, the heterogeneous reactions of trace gases in the atmosphere on atmospheric particles has become increasingly important (Ravishankara, 1997), because they not only account for the alteration of the particulate composition and its surface properties (Aubin and Abbatt, 2006; Jang et al., 2002) but also affect the sources and sinks of trace gases (Jacob, 2000). Several atmospheric modeling studies have shown that atmospheric particles often acting as a sink for certain species (Dentener et al., 1996; Usher et al., 2003b). A major contributor to the loading of atmospheric particles is mineral dust, which mainly originates from arid and semi-arid regions with global source strength of about 1000-3000 $Tg \cdot yr^{-1}$ (Dentener et al., 1996).

The surface oxygen, hydroxyl group, absorbed water and defect sites on mineral oxides may provide reactive sites for the heterogeneous uptake of trace gases. Recently, using infrared spectroscopy, a few researchers have reported the heterogeneous reactions mechanism of OCS on atmospheric particles, and mineral oxides including Al_2O_3, SiO_2, Fe_2O_3, CaO, MgO, MnO_2 and the mixture of Fe_2O_3 and NaCl (Chen et al., 2007; He et al., 2005; Liu et al., 2006, 2007a, 2007b, 2009a; Wu et al., 2004, 2005). In these studies, hydrogen thiocarbonate ($HSCO_2^-$) was found as a key intermediate (He et al., 2005; Liu et al., 2006, 2007a, 2007b, 2009a). Gaseous carbon dioxide (CO_2) and surface sulfate (SO_4^{2-}) were found to be the gaseous and surface products (Chen et al., 2007; He et al., 2005; Liu et al., 2006, 2007a, 2007b, 2009a), respectively. Surface sulfite and element sulfur (Wu et al., 2004, 2005) were also observed as surface sulfur species. Additionally, gaseous hydrogen sulfide (H_2S) was detected as one of the hydrolysis products for the heterogeneous reaction of COS on MgO and Al_2O_3 (Liu et al., 2007a, 2008a, 2008b, 2009b). The previous works demonstrate that heterogeneous reactions on mineral dust may be a potential sink for OCS in the troposphere. However, besides on Al_2O_3 and MgO, the reactions on all of the other oxides were mainly investigated using infrared spectroscopy with a high OCS concentration. Thus, the reaction pathway on these mineral oxides still needs to be further identified by other experimental methods. In particular, the difference in reaction pathway on these oxides is unclear. On the other hand, the significance of these reactions on the global chemical cycle of OCS depends on its reaction rates or uptake coefficients. However, at present day, the uptake coefficients of OCS on the

typical mineral oxides are very limited. Therefore, the kinetic study for the heterogeneous reactions of OCS on mineral dust is necessary.

In this study, besides α-Al_2O_3 and MgO as reported previously (Liu et al., 2008a, 2008b, 2009b), we further investigated the heterogeneous reactions of OCS on the typical mineral oxide components in atmospheric particles, including SiO_2, CaO, α-Fe_2O_3, ZnO, and TiO_2, using a Knudsen cell reactor and a diffuse reflectance UV-vis spectroscopy. To facilitate comparison, the results of α-Al_2O_3 and MgO were also included. It revealed that the reactions could readily take place on some mineral oxides and some differences in reaction pathway exist on these oxides. On the basis of the uptake coefficients measured by Knudsen cell reactor, the environmental implications were discussed.

2. Experimental Section

2.1. Materials. All of the chemicals were used with received. These included: Carbonyl sulfide (OCS, 1.98%, OCS/N_2, Scott Specialty Gases Inc.), N_2 and O_2 (99.99% purity, Beijing AP Beifen Gases Inc.), and C_2H_5OH (99.7%, Beijing Chemicals Factory).

According to the main composition of authentic mineral dust (He et al., 2005) and the upper continental crust (Usher et al., 2003a), SiO_2, α-Al_2O_3, CaO, MgO, α-Fe_2O_3, ZnO, and TiO_2 were chose as model dust samples. α-Al_2O_3 was prepared through calcining AlOOH (Shandong Alumina Corpartion) at 1473 K for 3 h. All of the other oxides are of analytic purity grade, including SiO_2 and TiO_2 (Beijing Yili Fine Chemicals Co. Ltd), α-Fe_2O_3 (Beijing Nanshang Chemicals Factory), CaO and

ZnO (Shantou Nongxi Chemicals Factory Guangdong), and MgO (Tianjin Hangu Haizhong Chemicals Factory).

2.2. Characterization of Sample. X-ray powder diffraction pattern was collected from 10 to 90° 2θ on a D/max-RB automatic powder X-ray diffractometer using Cu Kα irradiation. Nitrogen Brunauer-Emmett-Teller (BET) physisorption measurement was performed with a Micromeritics ASAP 2000 analyzer.

2.3. Experimental Methods. *KCMS experiment*. A Knudsen cell reactor coupled to a quadrupole mass spectrometer (KCMS, Hiden, HAL 3F PIC) was used to study the reaction pathway and to measure the uptake coefficients of OCS on the mineral oxides. The apparatus was described detailedly elsewhere (Liu et al, 2008a, 2008b). Briefly, the mass spectrometer was housed in a vacuum chamber equipped with a 300 $L \cdot s^{-1}$ turbomolecular pump (Pfeiffer) and an ion gauge (BOC Edward). The vacuum chamber between the quadrupole mass spectrometer (QMS) and the Knudsen cell reactor was pumped by a 60 $L \cdot s^{-1}$ turbomolecular pump for differential pumping of the mass spectrometer and an ion gauge (both from BOC Edward).The Knudsen cell reactor consists of a stainless steel chamber with a gas inlet controlled by a leak valve, an escape aperture whose area could be adjusted with an adjustable iris and a sample holder attached to the top ceiling of a circulating fluid bath. The sample in the sample holder can be exposed or isolated to the reactants by a lid connected to a linear translator.

The oxide samples were dispersed evenly on the sample holder with alcohol and then dried at 393 K for 2 h. The pretreated samples and the reactor chamber were

112 evacuated at 323 K for 6 h to reach a base pressure of approximately 5.0×10^{-7} Torr.
113 After the system was cooled to 300 K, the sample cover was closed. 1.51 % of OCS
114 gas balanced with simulated air (21% O_2 and 79% N_2) was introduced into the reactor
115 chamber through a leak valve. The relative humidity in the reactant gases was
116 measured to be 7% using a hygrometer (Center 314) with a relative error of ±1.5%.
117 The pressure in reactor was measured using an absolute pressure transducer. Prior to
118 the experiments, the reactor chamber was passivated with OCS in air for 150 min to a
119 steady state of QMS signal established as the oxide samples were isolated from the
120 gas by the sample cover. Uptake measurements on all samples were obtained with an
121 average OCS partial pressure of $5.3\pm0.3\times10^{-6}$ Torr, which was equivalent to
122 $1.7\pm0.2\times10^{11}$ molecules·cm^{-3} or 7.0±0.3 ppbv. The uptake coefficients were calculated
123 based on the KCMS signal. According to the pressure in the vacuum chamber and the
124 pumping speeds of turbomolecular pumps, the mass signal intensity of OCS could be
125 converted to flow rate of molecules into the reactor. Then adsorption capacity of OCS
126 on mineral oxides could be calculated from the integrated area of a flow rate of
127 molecules into the reactor versus time.

128 *UV-vis experiment*. The surface sulfur species on oxides after heterogeneous
129 reaction with OCS were identified using a diffuse reflectance UV-vis
130 Spectrophotometer (U-3310, Hitachi). 100 mg of mineral oxides in quartz tube were
131 exposed to 1000 ppmv of OCS/air in the flow of 100 mL·min^{-1} for 9 h at 300 K, and
132 then the UV-vis spectra were collected promptly using the corresponding pure oxides
133 as reference samples.

3. Results and Discussion

3.1. Characterizations. XRD results indicate that these oxides used in experiment are quartz (SiO_2), corundum (α-Al_2O_3), lime (CaO), hematite (MgO), periclase (α-Fe_2O_3), spartalite (ZnO), and anatase (TiO_2), respectively. The detailed information was described elsewhere (Liu et al., 2008b). Because of the strong basicity and hygroscopicity, CaO sample contains a small amount of $Ca(OH)_2$.

The surface areas of these oxides are almost in the same order and close to the value of the authentic atmospheric particles (He et al., 2005) as shown in Table 1.

3.2. Uptake of OCS and desorption behavior of surface species on mineral oxides. *α-Al_2O_3 and MgO.* In our previous works (Liu et al., 2005, 2006, and 2008a), we have reported the hydrolysis reaction and oxidation pathways of OCS on Al_2O_3. To facilitate comparison, the Knudsen cell results on α-Al_2O_3 and MgO were also described here briefly and shown in Figs. 1S and 2S. As shown in Fig. 1S, the consumption of OCS and desorption of CO_2 and H_2S after reaction could be seen clearly when 50.2 mg α-Al_2O_3 was exposed to $5.3\pm0.3\times10^{-6}$ Torr at 300 K. Fig. 2s shows the heterogeneous reaction of OCS on 100.0 mg of MgO at 300 K. As shown in Fig. 2S, the uptake of OCS (m/e=60) was companied by the production of CO_2 (m/e=44) and H_2S (m/e=34) on MgO. Based on the discussion in previous work (Liu et al., 2006, 2007a, 2008a, 2009a; He et al., 2005; Wu et al., 2004, 2005), we can conclude that hydrolysis and oxidation reactions of OCS occurred on α-Al_2O_3 and MgO.

CaO. Figure 1 shows the heterogeneous reactions of OCS on 100.4 mg of CaO at

300 K, respectively. Although CaO is also a type of *FCC* crystalline of alkaline earth oxide as same as MgO, the uptake profiles of OCS on CaO were quite different from that on MgO as shown in Fig. 2S. They are also different from that on α-Al_2O_3 (Fig. 1S). The uptake of OCS on CaO was accompanied by the production of CO_2, while no formation of H_2S was detected. In our previous work (Liu et al., 2007b), surface CO_3^{2-}, HCO_3^-, SO_4^{2-}, and SO_3^{2-} were observed while no surface HS was observed for the heterogeneous reaction of OCS on CaO using *in situ* DRIFTS. In addition, except for CO_2, no desorptions of OCS and H_2S were observed in the *in situ* desorption experiment as shown in Fig. 1(D-F). These results suggest that the reaction pathway of OCS on CaO might be different from that on MgO and α-Al_2O_3. However, it should be pointed out that if H_2S produced by heterogeneous reaction on the surface of oxides can be easily and quickly transformed into other species, it is hard to detect the surface HS or gaseous H_2S in DRIFTS and KCMS experiments.

α-Fe_2O_3 and ZnO. Figures 2 and 3 show the heterogeneous uptake of OCS and desorption of surface species on 141.3 mg of α-Fe_2O_3 and 200.9 mg of ZnO at 300 K, respectively. As the sample cover was opened, the mass signal intensity of OCS (m/e=60) decreased dramatically on both of these two samples (Figs. 2A and 3A). Although the total surface areas of α-Fe_2O_3 and ZnO used in this experiment were lower than that of α-Al_2O_3, MgO, and CaO, the dropping amplitude for the relative intensity of OCS in Figs. 2A and 3A were much larger than that in Figs. 1S, 2S and 1. However, the signal intensity of OCS quickly recovered to its baseline within 10 min. It suggests that the active sites for effectively uptaking OCS onto α-Fe_2O_3 and ZnO

178 are very abundant, while they have lower catalytic reactivity for OCS hydrolysis or
179 oxidation. In Figs. 2 and 3, the increasing of signal intensity for CO_2 was very weak
180 and the change of signal intensity for H_2S was also negligible. In the end of uptake
181 experiment, as for α-Fe_2O_3, desorption of OCS was very distinct (Fig. 2D), while
182 desorption of CO_2 was very weak (Fig. 2E) and no desorption of H_2S (Fig. 2F) was
183 observed. For ZnO, no desorptions of OCS, CO_2, and H_2S were observed as shown in
184 Fig. 3(D-F) even when the escape hole was increased to its upper limit. Therefore,
185 these results suggest that OCS might be reversibly adsorbed on α-Fe_2O_3 and
186 irreversibly adsorbed on ZnO. In order to confirm these processes, the repeated uptake
187 experiments were further carried out on ZnO and α-Fe_2O_3. After the uptake
188 experiment finished, the samples were outgassed at $3.0\pm1.0\times10^{-7}$ Torr and at 300 K
189 for 18 h. Then repeated uptake experiments were performed at 300 K. As can be seen
190 from the Fig.3S, adsorption of OCS on ZnO was very clear in the 1st run, while it
191 became very weak in the 2nd and the 3rd runs. For the comparison experiment, OCS
192 could reversibly adsorb on α-Fe_2O_3. These results confirmed the reversible adsorption
193 of OCS on α-Fe_2O_3 and irreversible adsorption on ZnO.

194 In our previous work, we found that when α-Fe_2O_3 and ZnO were exposed to
195 OCS at 303 K for a long time (120 min), the consumption of surface hydroxyl was
196 prominent and accompanied by the very weak absorbance of $HSCO_2^-$, HCO_3^-, and
197 SO_4^{2-} etc. (Liu et al., 2007b). Recently, Chen et al. (2007) also observed the
198 consumption of OCS on α-Fe_2O_3 for 24 h, while the reaction rate constant was
199 measured to be very low. It should be noted that in these previous works (Chen et al.,

200 2007; Liu et al., 2007b), the uptake experiments were investigated using DRIFTS
201 reactors with a long exposure time. Thus, they obtained the integrated signals for the
202 reaction on α-Fe_2O_3, while the differential signals was gained within a 0.6 s time-scale
203 in this work. Therefore, the uptake experiments performed in Knudsen cell reactor
204 represent more initial and fresh state for oxides. Because the reactions of OCS on
205 α-Fe_2O_3 and ZnO were also found to be very slow even though in the DRIFTS
206 reactors, according to uptake experiments performed in this work, we think that OCS
207 should be mainly reversibly adsorbed on α-Fe_2O_3 and irreversibly adsorbed on ZnO,
208 and the hydrolysis and oxidation reactions on them are negligible.

209 *SiO_2 and TiO_2.* The uptake profiles of OCS on SiO_2 and TiO_2 are shown in Fig. 4.
210 When 350.5 mg of SiO_2 and 400.0 mg of TiO_2 were exposed to the feed gas,
211 respectively, no uptakes of OCS were observed in Figs. 4A and 4D. The changes of
212 CO_2 and H_2S were also negligible when the sample cover was opened. In our previous
213 work, we had observed the consumption of OCS over SiO_2 and TiO_2 in closed system
214 were faintly faster than that over the background of *in situ* DRIFTS reactor chamber
215 (Liu et al., 2007b). As discussed above, the difference between KCMS experiments
216 and *in situ* DRIFTS experiments is derived from the different experimental methods.
217 KCMS is a differential reactor, when the change of the flow rate of OCS in the reactor
218 is lower than 2×10^{14} molecules·s^{-1} (3σ), the QMS can not detect any change of its
219 signal intensity, while the *in situ* DRIFTS reactor chamber in the closed system
220 belongs to an integrated reactor, and the consumption of OCS is the accumulation of
221 infrared signal at several minutes or several hours level. Therefore, we can conclude

222 that even though the heterogeneous reactions of OCS can take place on SiO_2 and TiO_2,
223 they are very slow and have little contribution to the sink of OCS in the troposphere.
224 **3.3 Identification of other surface species and reaction pathway.** Using DRIFTS,
225 we have identified the surface species including $HSCO_2^-$, HS, CO_3^{2-}, HCO_3^-, SO_3^{2-},
226 and SO_4^{2-} etc. for the hydrolysis and oxidation of OCS on most of these oxides (He et
227 al., 2005; Liu et al., 2006, 2007a, 2007b, 2009a). Wu et al. (2004, 2005) also observed
228 the formation of element sulfur by XPS. In order to identify other surface species
229 during heterogeneous reactions and to further clarify the difference between the
230 reaction pathway of OCS on CaO and that on MgO (as shown in Figs. 1 and 2S), the
231 surface sulfur containing species were investigated by diffuse reflectance UV-vis
232 spectroscopy. After the CaO and MgO samples were exposed to 1000 ppmv of
233 OCS/air in 100 mL/min at 300 K for 9h, the diffuse reflectance UV-vis spectra were
234 collected immediately using the corresponding pure oxides as reference samples. The
235 UV-vis spectra are shown in Fig. 5. The peak at 217 nm is assigned to surface HSO_3^-,
236 and the peak at 226 nm is ascribed to surface S^{2-} (Davydov, 2003). The abroad bands
237 around 260-280 nm, and 340 nm were also observed and are assigned to the
238 absorbance bands of element sulfur (Davydov, 2003).
239 As can be seen in Fig. 5, surface HSO_3^- and S^{2-} are the common surface sulfur
240 containing species for the heterogeneous reaction of OCS on both CaO and MgO. The
241 formation of HSO_3^- is well supported by the DRISFTS results (He et al., 2005; Liu et
242 al., 2006, 2007a, 2007b, 2009a). In Fig. 5A, very strong broad bands attributing to
243 element sulfur were observed on CaO, which means element sulfur should also be one

244 of the surface products for the heterogeneous reaction of OCS on CaO. It should be
245 noted that S^{2-} were also observed for the OCS treated CaO sample. Therefore, we
246 postulate that element S might be the further oxidization product of S^{2-}, while S^{2-} is
247 result from the decomposition of H_2S or surface HS. This assumption is accordance
248 with no desorption of H_2S after heterogeneous reaction of OCS on CaO (Fig. 3F).
249 Additionally, after heterogeneous reaction, the sample was purged further with pure
250 O_2 for 9 h and the absorbance of elemental sulfur decreased greatly (not shown). It
251 means the newly formed sulfur can be further oxidized to high state species. As for
252 MgO, although element S can be also observed (Fig. 5B), its relative content was
253 much lower that that on CaO. It implies a low decomposition rate of surface HS to S
254 on MgO, thus the formation and desorption of H_2S was very prominent (Fig. 2S), and
255 the surface HS was also observable in the *in situ* infrared spectra (Liu et al., 2007a).
256 As for OCS treated α-Fe_2O_3 and ZnO, the UV-vis signal (not shown) was very weak
257 due to their low reactivity.

258 According to perturbation theory and orbital mixing, the decomposition reactivity
259 of H_2S on mineral oxides was found to be related to the band gap of oxides. The lower
260 the band gap of the oxide, the higher the adsorption activity and decomposition
261 reactivity of H_2S (Rodriguez et al., 1998). The band gap of CaO is 6.8 eV, while it is
262 7.7 eV for MgO (Baltache et al., 2004). It suggests that the decomposition reaction of
263 H_2S on CaO should be more facile than that on MgO. Therefore, we can deduce that
264 the absence of H_2S in the products for the heterogeneous reaction of OCS on CaO
265 should be ascribed to the formation of CaS and element sulfur on the surface.

It should be noted that Fe and Zn are typical sulphophile elements. It has been found that H_2S undergoes complete decomposition on ZnO to form sulfide at 300 K (Lin et al., 1992; Rodriguez et al., 1998). On the other hand, the small band gap of ZnO (3.4 eV) (Rodriguez et al., 1998) also implied its strong decomposition ability for H_2S to surface sulfide or sulfur species. As for α-Fe_2O_3, the band gap is 2.2 eV, which means the stronger decomposition ability for H_2S to surface sulfide or sulfur species. However, in our previous work, we have found that reactivity of OCS on mineral oxides depends on the basicity of oxides, i. e., the stronger the basicity of oxide, the higher the reactivity of OCS on it (Liu et al., 2007b and 2009b). α-Fe_2O_3 and ZnO are typical acidic oxides, which suggests very low heterogeneous reactivity. On the other hand, in Figs. 2 and 3, desorption of CO_2 on α-Fe_2O_3 and ZnO was negligible, which suggests the amount of H_2S produced in heterogeneous reaction should be negligible. In particular, the reversible adsorption of OCS on α-Fe_2O_3 was observed in Fig. 2. Therefore, even if hydrolysis of OCS could occur on α-Fe_2O_3 and ZnO, the surface sulfide or element sulfur species, which is easily formed on these oxides, should lead to the quick deactivation by blocking the active site for the heterogeneous reaction of OCS on α-Fe_2O_3 and ZnO. Thus, the oxides with stronger basicity and lower decomposition ability for H_2S to surface sulfide or element sulfur species should show higher catalytic activities for decomposition of adsorbed OCS than these oxides with the anti-properties. Thus the main heterogeneous process of OCS on α-Fe_2O_3 and ZnO may be the adsorption process and the catalytic reaction of OCS is less important.

Based on above results and the previous works (Chen et al., 2007; He et al., 2005; Liu et al., 2006, 2007a, 2007b, 2009), the reaction pathway for OCS on mineral oxides was summarized in Scheme 1. Catalytic reactions are very obvious on MgO, CaO and α-Al_2O_3. The key intermediate of $HSCO_2^-$ can be directly oxidized to HSO_3^-, HCO_3^-, and SO_4^{2-}. It can also hydrolyze to form H_2S and CO_2. Gaseous H_2S can further decompose to sulfide compound (MS) and element sulfur on MgO and CaO. The surface sulfur species including sulfur, sulfide and sulfite can be finally oxidized to sulfate. Irreversible adsorption of OCS on ZnO and reversible adsorption of OCS on α-Fe_2O_3 can take place at 300 K. As for TiO_2 and SiO_2, no uptake of OCS was observed.

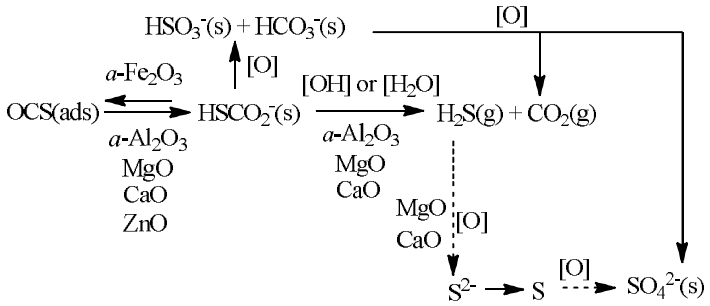

Scheme 1. Reaction pathway for OCS on different mineral oxides.

3.4. Reaction kinetics for the heterogeneous reaction of OCS on mineral oxides.

Uptake coefficient, which demonstrates the activity of adsorption or reaction for heterogeneous process, was the most commonly used kinetic parameter in atmospheric chemistry and also in the model studies. It was defined by Eq. 1 (Underwood et al., 2000).

$$\gamma = \frac{-\frac{dn}{dt}}{\omega} \qquad (1)$$

where $-\frac{dn}{dt}$ is the number of molecules lost from the gas phase per second due to the collision between gas molecules and solid surface (molecules·s^{-1}); ω is the total number of gas-surface collisions per second. Based on the Knudsen cell experimental results, the observed uptake coefficients, γ_{obs}, of OCS on mineral oxides characterized by the loss of gaseous OCS can be calculated from Knudsen cell equation (Barone et al., 1997; Beichert and Finlayson-Pitts, 1996; Liu et al., 2008a, 2008b; Underwood et al., 2000).

$$\gamma_{obs} = \frac{A_h}{A_s}\frac{(I_0 - I)}{I} \quad (2)$$

where, A_h is the effective area of the escape aperture (cm^2); A_s is the geometric area of the sample holder (cm^2); and I_0 and I are the mass spectral intensities of OCS with the sample holder closed and open, respectively. If the reactant gas can diffuse into the underlying layers for the multilayer powder sample, the effective collision area should be considered. Usually, the effective surface area was used. And then the true uptake coefficients, γ_t (BET), can be calculated from

$$\gamma_t = slope \cdot \left(\frac{A_s}{S_{BET}} \right) \quad (3)$$

where *slope* is the slope of plot of γ_{obs} and sample mass in linear region (mg^{-1}); S_{BET} is the specific surface area of particle sample (cm^2·mg^{-1}) (Carlos-Cuellar et al., 2003).

The observed uptake coefficients calculated according to the geometric area of the sample holder at initial time (referred as γ_{obs}(Initial)) and at steady state (γ_{obs}(Steady state)) were plotted along with sample mass through the origin and are shown in Fig. 6(A-C). As for α-Fe_2O_3 and ZnO, γ_{obs}(Initial) and adsorption capacities

were given in Figs. 6D and 6E. The error bar was 15 % obtained from the repeated experiments. It can be seen from Fig. 8 that there was a strong linear dependence of γ_{obs} or adsorption capacity versus sample mass for all tested mineral oxides. It means the underlying layers of these oxide samples also contribute to the heterogeneous uptake and catalytic reaction under this experimental conditions. Therefore, γ_t(BET) can be calculated from the slope and specific area of oxides sample via Eq. 3. The γ_t(BET) of OCS on different oxides were presented in Table 1 and in the range of 10^{-7}-10^{-8}. The γ_t(Initial) were in the order: α-Fe_2O_3 > ZnO > CaO > α-Al_2O_3 > MgO > SiO_2, TiO_2, while the order of γ_t(Steady state) is MgO > α-Al_2O_3, CaO > ZnO, α-Fe_2O_3, SiO_2, TiO_2.

When the intensity of mass spectrometer for OCS was corrected with flow rate of molecules and the consumption of OCS by catalytic reaction was subtracted, the adsorption capacity of OCS on different oxides was calculated and shown in Table 1. As can be seen in Table 1, the values of initial uptake coefficients of OCS on α-Al_2O_3, MgO, CaO, α-Fe_2O_3, and ZnO were much greater than that of steady state uptake coefficients. In despite of large initial uptake coefficients for α-Fe_2O_3 and ZnO, their steady state uptake coefficients decreased to zero. As discussed above, the initial uptake was mainly due to the adsorption process, while the steady state uptake was related to the catalytic reaction. It means that only a part of adsorbed OCS can be transformed to $HSCO_2^-$, and then it decomposes into CO_2 and H_2S. The decomposition of $HSCO_2^-$ is the rate determine step (Liu et al., 2008b). On the other hand, the surface species such as HCO_3^-, CO_3^{2-}, S^{2-}, S, SO_3^{2-}, and SO_4^{2-} also induced

349 the decline of catalytic reactivity. Therefore, the initial uptake coefficients on all of
350 these oxides are much higher than their steady state uptake coefficients. Among these
351 surface species, sulfide species have a very prominent effect, especially on ZnO, and
352 CaO. Although the initial uptake coefficients were very large on these oxides, the
353 steady state uptake coefficients (shown in Table 1) were very small because the
354 sulfide or sulfur species could hardly desorb from the surface. In addition, as
355 mentioned above, the heterogeneous reactivity of OCS on mineral dust is in relation
356 to the surface basicity of oxides (Liu et al., 2007b and 2009b). The order of steady
357 state uptake coefficients also supports the forenamed assumption. Except for CaO,
358 which is related to the deactivation of surface sulfur species, the order of steady state
359 uptake coefficients is almost the same as the basicity sequence of mineral oxides.
360 Therefore, we can deduce that the alkali elements and alkaline-earth metals in the
361 authentic atmospheric particles should promote the heterogeneous reaction of OCS in
362 the troposphere.

363 According to the true uptake coefficients of single oxide and the mineral
364 composition of authentic atmospheric particulate matter (He et al., 2005; Usher et al.,
365 2003a), the true uptake coefficient of authentic atmospheric mineral dust can be
366 estimated from

367 $$\gamma_{dust} = \sum f_i \gamma_i \quad (4)$$

368 where γ_{dust} is the true uptake coefficient for mineral dust; f_i is the fraction of oxide
369 in atmospheric mineral dust (He et al., 2005); γ_i is the true uptake coefficient of
370 corresponding oxide (Usher, et al., 2002). The γ_{dust} was calculated to be from

371 3.84×10^{-7} (initial) to 2.86×10^{-8} (steady state). This value is comparable to the uptake
372 coefficient of NO_2 on mineral dust (10^{-7}-10^{-8}) (Ullerstmal et al., 2003; Underwood, et
373 al., 1999, 2000).

374 In our previous work (Liu et al., 2007b), we have found that the heterogeneous
375 reaction of OCS on mineral oxides is a first-order reaction. Therefore, the reaction
376 rate constant can be calculated from Eq. 5 (Ravishankara, 1997).

377 $$k_{dust} = \frac{\bar{v} \cdot \gamma_{dust} \cdot SA}{4} \qquad (5)$$

378 Here, k_{dust} is the rate constant for the first-order reaction (s^{-1}); $\bar{v}$ is the average
379 velocity of OCS molecules ($m \cdot s^{-1}$); γ_{dust} is the true uptake coefficient of mineral dust
380 ($m^2 \cdot m^{-3}$); SA is the globally-averaged dust surface area (150 $\mu m^2 \cdot cm^{-3}$) (de Reus et al.,
381 2000; Frinak et al., 2004). The rate constants of OCS on mineral dust in the
382 troposphere were estimated to be 4.69×10^{-9} s^{-1} (initial) and 3.49×10^{-10} s^{-1} (steady
383 state).

384 **4. Conclusions and atmospheric implications**

385 In this work, the heterogeneous reactions of OCS on the typical mineral oxides
386 were investigated by using Knudsen cell reactor and diffuse reflectance UV-vis
387 spectroscopy. Catalytic hydrolysis and oxidation were observed on MgO, CaO and
388 α-Al_2O_3. Reversible adsorption of OCS on α-Fe_2O_3 and irreversible adsorption on
389 ZnO were observed. As for TiO_2 and SiO_2, no uptake of OCS was observed. For CaO,
390 the decomposition reactivity of hydrolysis product (H_2S) is stronger than that on MgO
391 and α-Al_2O_3, which leads to the obvious deactivation of hydrolysis of OCS on CaO at
392 steady state. The uptake coefficients (BET) of OCS on these oxides were measured to

393 be in the range of 10^{-7}-10^{-8}, and are comparable with the uptake of NO_2 on mineral
394 dust.

395 Because the initial uptake is mainly due to adsorption, the heterogeneous process
396 of OCS on mineral dust could be divided into adsorption and catalytic reaction. In the
397 real atmosphere, the uptake coefficients at steady state should be more representative
398 than the initial uptake coefficients because once emitted into the atmosphere the fresh
399 dust samples were often quickly aged by reactant gases. With the assumption of the
400 total OCS mass of 4.63 Tg in the troposphere (Chin and Davis, 1995), and the
401 first-order reaction rate constants of OCS on mineral dust (steady state), the global
402 flux of OCS on mineral dust due to heterogeneous reactions was calculated to be 0.05
403 $Tg \cdot yr^{-1}$. Thus, this value, which is relating to the catalytic activity of dust, is very
404 important to access the sinks of OCS due heterogeneous reaction.

405 Based on the adsorption capacity of each oxide and the mass fraction of oxide in
406 atmospheric mineral dust, the equivalent adsorption capacity of mineral dust was
407 calculated to be 8.00×10^{17} $molecules \cdot g^{-1}$ based on Eq. 6.

408 $$Ac_{dust} = \sum_i f_i Ac_i \qquad (6)$$

409 Where Ac is the adsorption capacity. The adsorption process might contribute the
410 global sink of 0.08-0.24 Tg $OCS \cdot year^{-1}$ with the deposit of mineral dust (1000-3000
411 $Tg \cdot year^{-1}$). Therefore, considering both the adsorption and the catalytic reactions, the
412 total sink of OCS due to mineral dust should be 0.13-0.29 $Tg \cdot year^{-1}$ via the adsorption
413 and catalytic reaction of mineral dust. Compared with other sinks, this value might be
414 equivalent to the annual flux for reaction of OCS with ·OH of 0.10 $Tg \cdot yr^{-1}$ (Watts,

2000). Even though only the consumption by catalytic reaction was considered, the contribution of mineral dust to the sink of OCS should also be not ignored.

Of course, the uptake coefficient of OCS on mineral dust estimated by using the uptake coefficients of OCS on the individual components and their mass fraction in the mineral dust (Eq.4) contains a considerable uncertainty. Therefore, in the future work, the uptake of OCS on realistic dust samples such as Sahara dust, Arizona Test dust or other authentic dust samples should be considered. On the other hand, the value of 150 $\mu m^2 \cdot cm^{-3}$ was taken from one flight airplane study (de Reus et al. 2000) and it is more representative of a regional dust layer rather than global average. Unfortunately, the global mean dust loading is unobtainable in published literatures. The estimating method for the sink of OCS due to heterogeneous reaction on mineral dust, therefore, is also a middle course of action. Additionally, the real atmosphere is very complicated. For example, the relative humidity and coexisting gases such as CO_2, NOx, SO_2, organic compounds, and alkali metal etc. may have a complex effect on the heterogeneous reaction of OCS on mineral dust. Our recent work (Liu et al., 2009b) demonstrates that adsorbed water on mineral oxides should restrict the heterogeneous reaction of OCS, while the basic membrane and the uncovered part by water still have catalytic activity. In addition, in this study, we did not consider the alkali metal (Na and K) in the oxides. However, our previous work found that strong basicity of oxide is in favor of the heterogeneous reaction of OCS. It means that the alkali metal should also promote this reaction. Therefore, our results in this study only present the case under clean and dry conditions. Whereas this study at least revealed

437 that heterogeneous reactions of OCS on mineral dust in the troposphere should be
438 considered for evaluating the atmospheric behavior of OCS.
439
440 **Acknowledgment.** This research was financially supported by the National Natural
441 Science Foundation of China (40775081, 20937004, and 50921064). Yongchun Liu
442 would also like to thank the President Scholarship of Chinese Academy of Sciences
443 for the financial support.
444
445 **References:**
446 Anderson, T. L.; Charison, R. J.; Schwartz, S. E.; Knutti, R.; Boucher, O.; Rodhe, H.;
447 Heintzenberg, J. Climate forcing by aerosols – a hazy picture. *Science*, 300,
448 1103-1104, **2003**.
449 Andreae, M. O.; Crutzen, P. J. Atmospheric aerosols: Biogeochemical sources and
450 role in atmospheric chemistry. *Science*, 276, 1052-1058, **1997**.
451 Aubin, D. G.; Abbatt, J. P. Laboratory measurements of thermodynamics of adsorption
452 of small aromatic gases to n-hexane soot surfaces. *Environ. Sci. Technol.*, 40,
453 179-187, **2006**.
454 Baltache, H.; Khenata, R.; Sahnoun, M.; Driz, M.; Abbar, B.; Bouhafs, B. Full
455 potential calculation of structural, electronic and elastic properties of alkaline
456 earth oxides MgO, CaO and SrO. *Phys. B*, 344, 334-342, **2004**.
457 Barone, S. B.; Zondlo, M. A.; Tolbert, M. A. A kinetic and product study of hydrolysis
458 of $ClONO_2$ on type Ia polar stratospheric cloud materials at 185 K. *J. Phys.*

Chem. A, 101, 8643-8652, **1997**.

Beichert, P.; Finlayson-Pitts, B. J. Knudsen cell studies of the uptake of gaseous HNO_3 and other oxides of nitrogen on solid NaCl: The role of surface-adsorbed water. *J. Phys. Chem.*, 100, 15218-15228, **1996**.

Carlos-Cuellar, S.; Li, P.; Christensen, A. P.; Krueger, B. J.; Burrichter, C.; Grassian, V. H. Heterogeneous uptake kinetics of volatile organic compounds on oxide surface using a Knudsen cell reactor: Adsorption of acetic acid, formaldehyde, and methanol on α-Fe_2O_3, α-Al_2O_3, and SiO_2. *J. Phys. Chem. A*, 107, 4250-4261, **2003**.

Chen, H. H.; Kong, L. D.; Chen, J. M.; Zhang, R. Y.; Wang L. Heterogeneous uptake of carbonyl sulfide on hematite and hematite-NaCl mixtures. *Environ. Sci. Technol.*, 41, 6484-6490, **2007**.

Chin, M.; Davis, D. D. A reanalysis of carbonyl sulfide as a source of stratospheric background sulfur aerosol. *J. Geophys. Res.*, 100, 8993-9005, **1995**.

Crutzen, P. J. The possible importance of CSO for the sulfate layer of the stratosphere. *Geophys. Res. Lett.*, 3, 73-76, **1976**.

Dentener, F. J.; Carmichael, G. R.; Zhang, Y.; Lelieveld, J.; Crutzen, P. J. Role of mineral aerosol as a reactive surface in the global troposphere. *J. Geophys. Res.*, 101, 22869-22889, **1996**.

de Reus, M.; Dentener, F.; Thomas, A.; Borrmann, S.; Ström, J.; Lelieveld, J. Airborne observations of dust aerosol over the North Atlantic Ocean during ACE 2: Indications for heterogeneous ozone destruction. *J. Geophys. Res.*, 105,

15263-15275, **2000**.

Frinak, E. K.; Wermeille, S. J. ; Mashburn, C. D. ; Tolbert, M. A. ; Pursell, C. J. Heterongeous reaciton of gaseous nitric acid on γ-phase iron(III) oxide. *J. Phys. Chem. A*, 108, 1560-1566, **2004**.

Graf, H. F. The complex interaction of aerosols and clouds. *Science*, 303, 1309-1311, **2004**.

He, H.; Liu, J. F.; Mu, Y. J.; Yu. Y. B.; Chen, M. X. Heterogeneous oxidation of carbonyl sulfide on atmospheric particles and alumina. *Environ. Sci. Technol.*, 39, 9637-9642, **2005**.

Hoggan, P. E.; Aboulayt, A.; Pieplu, A.; Nortier, P.; Lavalley, J. C. Mechanism of COS hydrolysis on alumina. *J. Catal.*, 149, 300-306, **1994**.

Isoniemi, E.; Pettersson, M.; Khriachtchev, L.; Lundell, J.; Räsänen, M. Infrared spectroscopy of H_2S and SH in rare-gas matrixes. *J. Phys. Chem. A*, 103, 679-685, **1999**.

Jacob, D. J. Heterogeneous chemistry and tropospheric ozone. *Atmos. Environ.*, 34, 2131-2159, **2000**.

Jang, M.; Czoschke, N. M.; Lee, S.; Kamens, R. M. Heterogeneous atmospheric aerosol production by acid-catalyzed particle reactions. *Science*, 298, 814-817, **2002**.

Jones, A.; Roberts, D. L.; Slingo, A. A climate model study of indirect radiative forcing by anthoropogenic sulphate aerosols. *Nature*, 370, 450-453, **1994**.

Lin, J. Y.; May, J. A.; Didziulis, S. V.; Solomon, E. I. Variable-energy photoelectron

503 spectroscopic studies of H2S chemisorption on Cu_2O and ZnO single-crystal
504 surfaces: HS- bonding to copper (I) and zinc (II) sites related to catalytic
505 poisoning. *J. Am. Chem. Soc.*, 114, 4718-4727, **1992**.
506 Liu, J. F.; Yu, Y. B.; Mu, Y. J.; He, H. Mechanism of heterogeneous oxidation of
507 carbonyl sulfide on Al_2O_3: An *in situ* diffuse reflectance infrared Fourier
508 transform spectroscopy investigation. *J. Phys. Chem. B*, 110, 3225-3230, **2006**.
509 Liu Y. C.; He, H. Heterogeneous reactivity of carbonyl sulfide on α-Al_2O_3 and
510 γ-Al_2O_3. *Atmos. Environ*., 42, 960-969, **2008a**.
511 Liu, Y. C.; He, H. Experimental and theoretical study of hydrogen thiocarbonate for
512 heterogeneous reaction of carbonyl sulfide on magnesium oxide. *J. Phys. Chem.*
513 *A*, 113, 3387–3394, **2009a**.
514 Liu Y. C.; He, H.; Ma, Q. X. Temperature dependence of the heterogeneous reaction
515 of carbonyl sulfide on magnesium oxide. *J. Phys. Chem. A*, 112, 2820-2826,
516 **2008b**.
517 Liu, Y. C.; He, H.; Xu, W. Q.; Yu, Y. B. Mechanism of heterogeneous reaction of
518 carbonyl sulfide on magnesium oxide. *J. Phys. Chem. A*, 111, 4333-4339, **2007a**.
519 Liu, Y. C.; Liu, J. F.; He, H.; Yu, Y. B.; Xue, L. Heterogeneous oxidation of carbonyl
520 sulfide on mineral oxides. *Chinese Sci. Bull.*, 52, 2063-2071, **2007b**.
521 Liu, Y. C.; Ma, Q. X.; He, H. Comparative study of the effect of water on the
522 heterogeneous reactions of carbonyl sulfide on the surface of α-Al_2O_3 and MgO.
523 *Atmos. Chem. Phys*., 9, 6273-6286, **2009b**.
524 Notholt, J.; Kuang, Z.; Rinsland, C. P.; Toon, G. C.; Rex, M.; Jones, N.; Albrecht, T.;

525 Deckelmann, H.; Krieg, J.; Weinzierl, C.; Bingemer, H.; Weller, R.; Schrems, O.
526 Enhanced upper tropical troposhperic COS: Impact on the stratospheric aerosol
527 layer. *Science*, 300, 307-310, **2003**.
528 Ravishankara, A. R. Heterogeneous and multiphase chemistry in the troposphere.
529 *Science*, 276, 1058-1065, **1997**.
530 Rodriguez, J. A.; Chaturvedi, S.; Kuhn, M.; Hrbek, J. Reaction of H_2S and S_2 with
531 metal/oxide surfaces: Band-gap size and chemical reactivity. *J. Phys. Chem. B*,
532 102, 5511-5519, **1998**.
533 Solomon, S.; Sanders, R. W.; Garcia, R. R.; Keys, J. G. Increased chlorine dioxide
534 over Antarctica caused by volcanic aerosols form Mount Pinatubo. *Nature*, 363,
535 245-248, **1993**.
536 Turco, R. P.; Whitten, R. C.; Toon, O. B.; Pollack, J. B.; Hamill, P. OCS, stratospheric
537 aerosols and climate. *Nature*, 283, 283-286, **1980**.
538 Ullerstam, M.; Johnson, M. S.; Vogt, R.; Ljungström, E. DRIFTS and Knudsen cell
539 study of the heterogeneous reactivity of SO_2 and NO_2 on mineral dust. *Atmos.*
540 *Chem. Phys*., 3, 2043-2051, **2003**.
541 Underwood, G. M.; Li, P.; Usher, C. R.; Grassian, V. H. Determining accurate kinetic
542 parameters of potentially important heterogeneous atmospheric reactions on solid
543 particles surfaces with a Knudsen cell reactor. *J. Phys. Chem. A*, 104, 819-829,
544 **2000**.
545 Underwood, G. M.; Miller, T. M.; Grassian, V. H. Transmission FT-IR and Knudsen
546 cell study of the heterogeneous reactivity of gaseous nitrogen dioxide on mineral

547 oxide particles. *J. Phys. Chem. A*, 103, 6184-6190, **1999**.
548 Usher, C. R.; Al-Hosney, H.; Carlos-Cuellar, S.; Grassian, V. H. A laboratory study of
549 the heterogeneous uptake and oxidation of sulfur dioxide on mineral dust
550 particles. *J. Geophys. Res.*, 107, 4713-4721, **2002**.
551 Usher, C. R.; Michel, A. E.; Grassian, V. H. Reactions on mineral dust. *Chem. Rev.*,
552 103, 4883-4939, **2003a**.
553 Usher, C. R.; Michel, A. E.; Stec, D.; Grassian, V. H. Laboratory studies of ozone
554 uptake on processed mineral dust. *Atmos. Environ.*, 37, 5337-5347, **2003b**.
555 Watts, S. F. The mass budgets of carbonyl sulfide, dimethyl sulfide, carbon disulfide
556 and hydrogen sulfide. *Atmos. Environ.*, 34, 761-779, **2000**.
557 West, J.; Wllianms, P.; Young, N.; Rhodes, C.; Hutchings, G. J. Low temperature
558 hydrolysis of carbonyl sulfide using γ-alumina catalysts. *Catal. Lett.*, 74, 111-114,
559 **2001**.
560 Wu, H. B.; Wang, X.; Cheng, J. M. Photooxidation of carbonyl sulfide in the presence
561 of the typical oxides in atmospheric aerosol. *Sci. China. Ser. B Chem.*, 48, 31-37,
562 **2005**.
563 Wu, H. B.; Wang, X.; Cheng, J. M.; Yu, H. K.; Xue, H. X.; Pan X. X.; Hou, H. Q.
564 Mechanism of the heterogeneous reaction of carbonyl sulfide with typical
565 components of atmospheric aerosol. *Chinese Sci. Bull.*, 49, 1231-1235, **2004**.
566
567
568

569

570 **TABLE 1.** Uptake coefficients and adsorption capacities of OCS on mineral oxides

Oxide	S_{BET} ($m^2 \cdot g^{-1}$)	Slope (mg^{-1})	Uptake coefficient (BET)		Adsorption capacity (molecules·g^{-1})
α-Al_2O_3	12.00	1.13±0.13E-5	Ini	4.95E-07	2.93E18
		1.62±0.27E-6	SS	7.10E-08	
MgO	14.59	1.34±0.17E-5	Ini	4.83E-07	4.62E18
		4.67±1.14E-6	SS	1.68E-07	
CaO	6.08	7.32±0.19E-6	Ini	6.33E-07	1.48E17
		8.89±2.02E-7	SS	7.69E-08	
α-Fe_2O_3	2.74	1.72±0.54E-5	Ini	3.30E-06	8.27E17
		0	SS	0	
ZnO	2.75	4.08±0.98E-6	Ini	7.80E-07	3.49E17
		0	SS	0	
SiO_2	4.80	0	Ini	0	0
TiO_2	12.74		SS	0	0
Mineral dust*	-	-	Ini	3.84E-07	8.00E17
			SS	2.86E-08	

Note: Ini - the initial uptake coefficient; SS – the steady state uptake coefficient at 30 min.

*The value for mineral dust was calculated based on the uptake coefficients of individual oxide and its fraction in authentic mineral dust.

571

572

573

574

575

576

577

578

579

580

581

582 **Figure Legends**

583 **Fig. 1.** The heterogeneous reaction of OCS on 100.4 mg of CaO at 300 K (left side)
584 and the *in situ* desorption of surface species in the end of uptake (right side).

585 **Fig. 2.** The heterogeneous reaction of OCS on 141.3 mg of α-Fe_2O_3 at 300 K (left side)
586 and the *in situ* desorption of surface species in the end of uptake (right side).

587 **Fig. 3.** The heterogeneous reaction of OCS on 200.9 mg of ZnO at 300 K (left side)
588 and the *in situ* desorption of surface species in the end of uptake (right side).

589 **Fig. 4.** The heterogeneous reactions of OCS on 350.5 mg SiO_2 and 400.0 mg TiO_2,
590 respectively. The left side is the uptake curve of OCS by SiO_2, and the right side is the
591 uptake curve of OCS by TiO_2.

592 **Fig. 5**. Diffuse reflectance UV-vis spectra of (A) CaO, and (B) MgO after exposed to
593 1000 ppmv of OCS in air for 9 h.

594 **Fig. 6.** The linear mass dependence between uptake coefficients or saturated
595 adsorption capacity and sample mass for OCS on mineral oxides at 300 K.
596 (A)α-Al_2O_3, (B) MgO, (C) CaO, (D) α-Fe_2O_3, (E) ZnO.

597

598

599

600

601

602

603

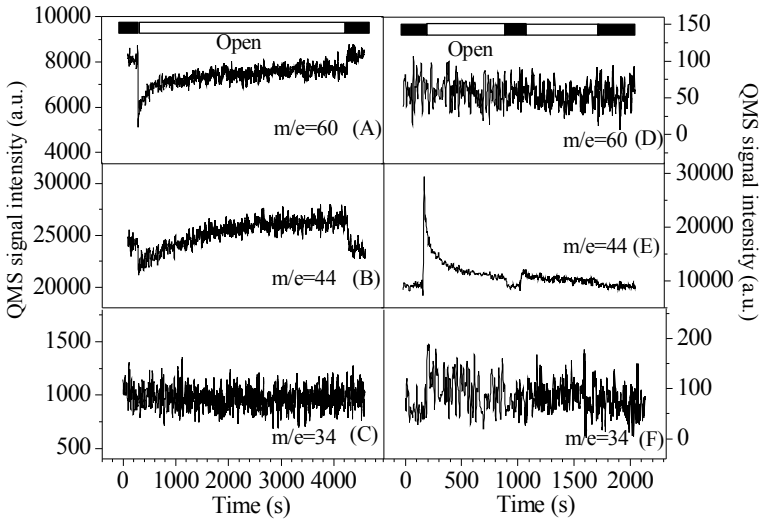

604

605 **Fig. 1.** The heterogeneous reaction of OCS on 100.4 mg of CaO at 300 K (left side)

606 and the *in situ* desorption of surface species in the end of uptake (right side).

607

608

609

610

611

612

613

614

615

616

617

618

619

620

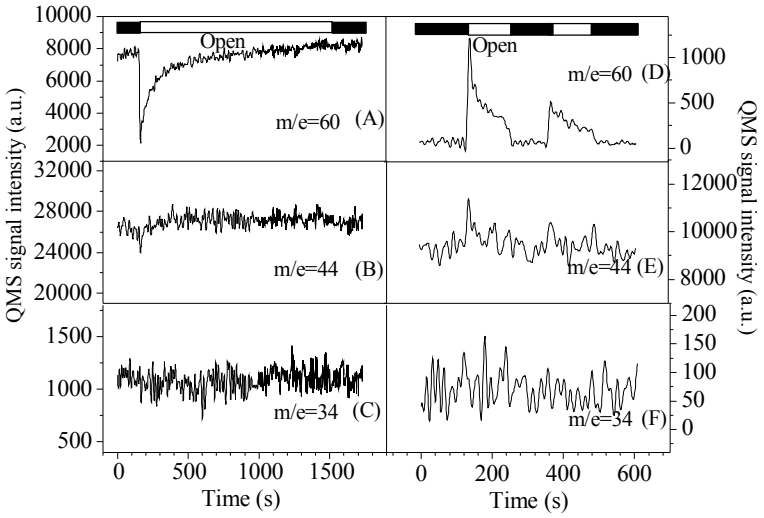

621

622 **Fig. 2.** The heterogeneous reaction of OCS on 141.3 mg of α-Fe_2O_3 at 300 K (left side)

623 and the *in situ* desorption of surface species in the end of uptake (right side).

624

625

626

627

628

629

630

631

632

633

634

635

636

637

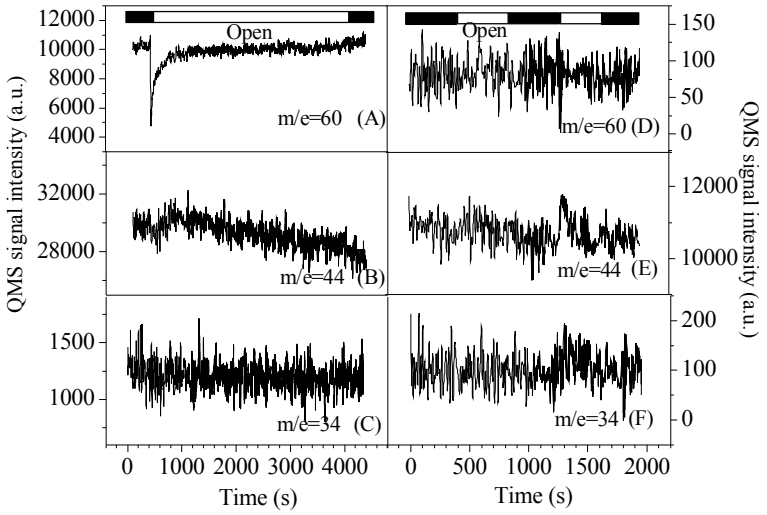

638

639 **Fig. 3.** The heterogeneous reaction of OCS on 200.9 mg of ZnO at 300 K (left side)

640 and the *in situ* desorption of surface species in the end of uptake (right side).

641

642

643

644

645

646

647

648

649

650

651

652

653

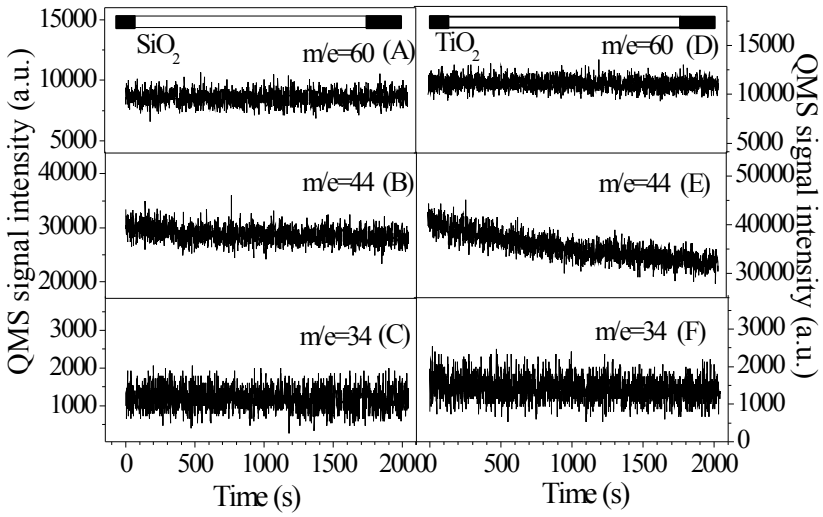

Fig. 4. The heterogeneous reactions of OCS on 350.5 mg SiO_2 and 400.0 mg TiO_2, respectively. The left side is the uptake curve of OCS by SiO_2, and the right side is the uptake curve of OCS by TiO_2.

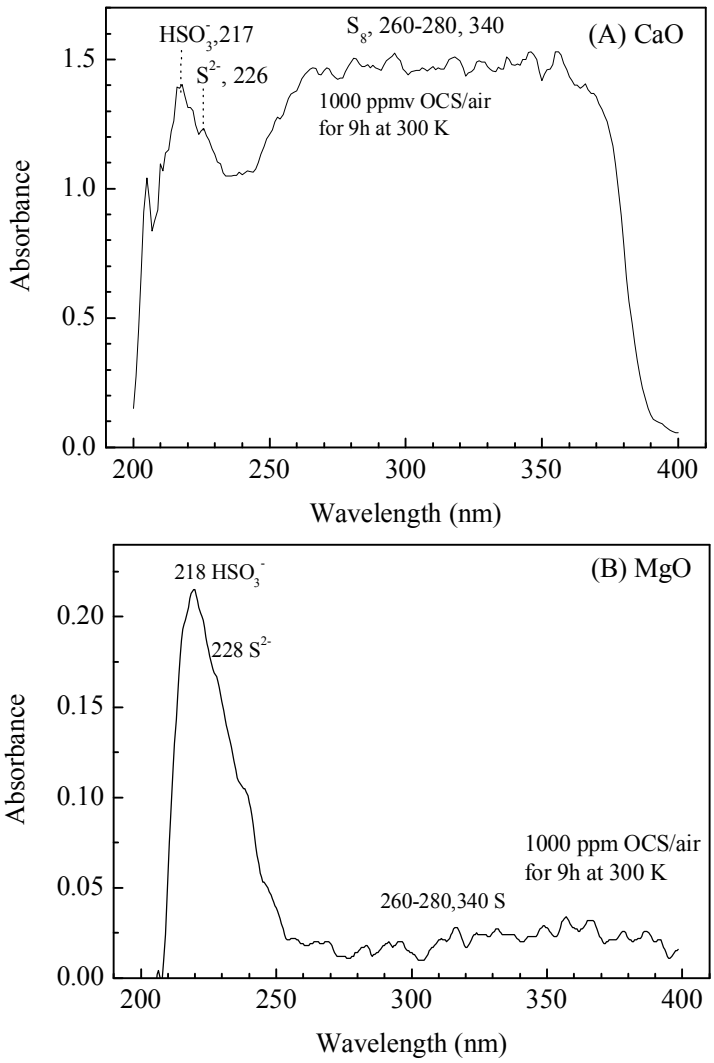

Fig. 5. Diffuse reflectance UV-vis spectra of (A) CaO, and (B) MgO after exposed to 1000 ppmv of OCS in air for 9 h.

681

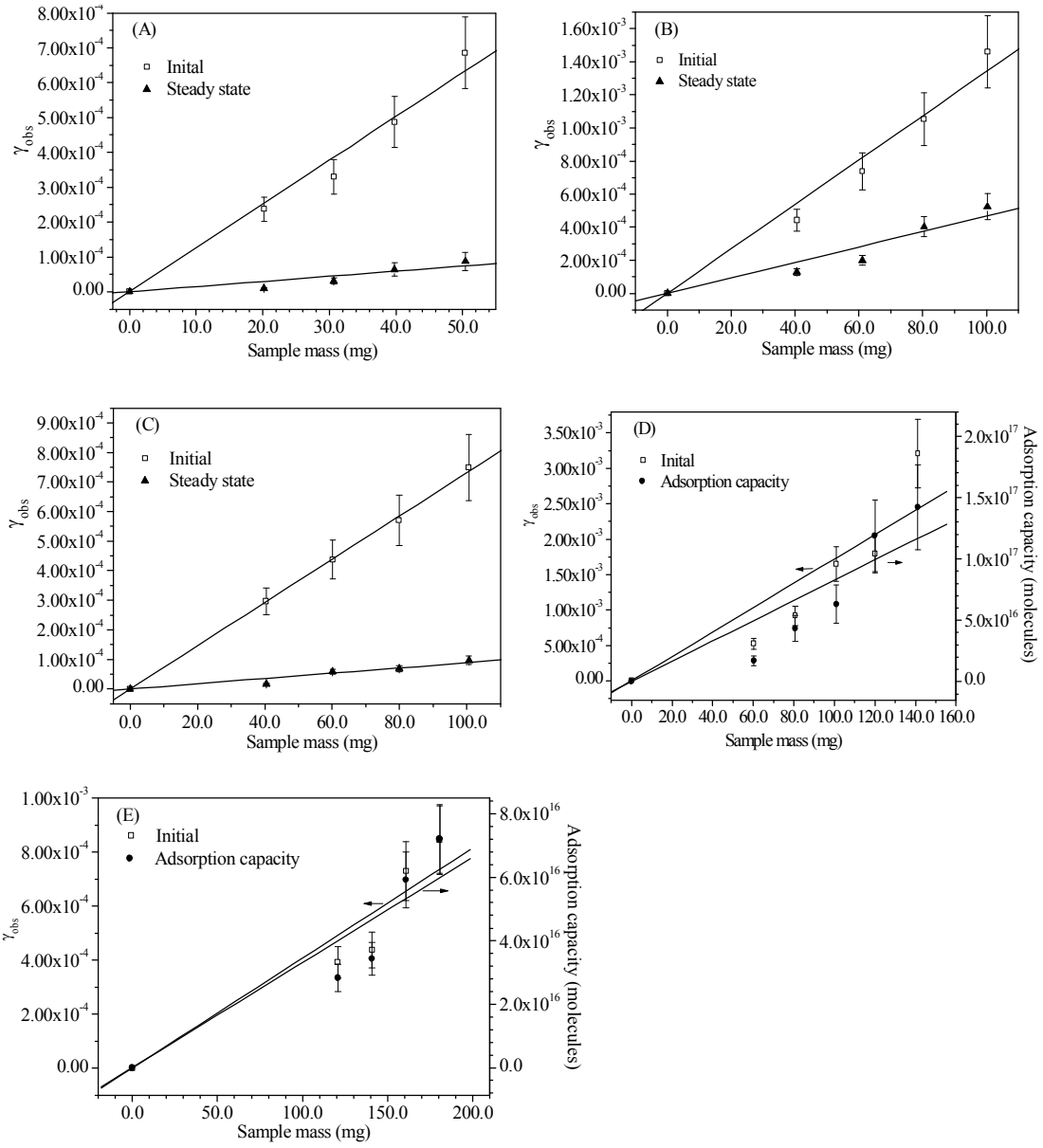

682

683

684

685 **Fig. 6.** The linear mass dependence between uptake coefficients or saturated

686 adsorption capacity and sample mass for OCS on mineral oxides at 300 K.

687 (A)α-Al_2O_3, (B) MgO, (C) CaO, (D) α-Fe_2O_3, (E) ZnO.

688

689

690

691

692 Supporting information:

693

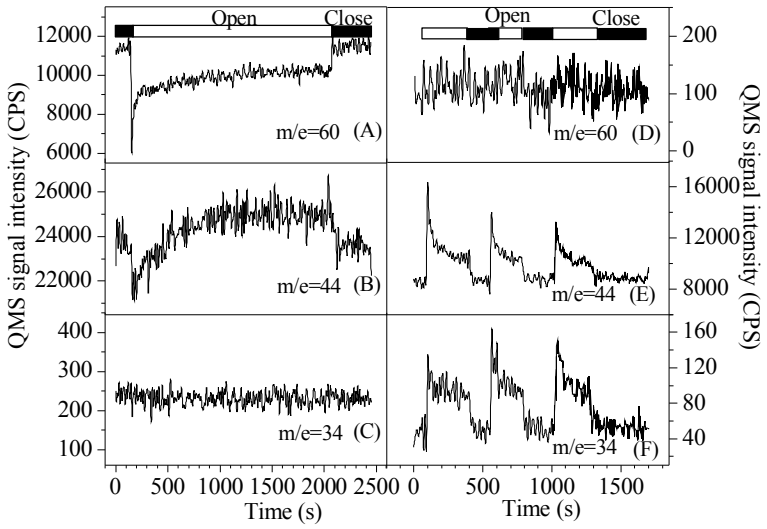

694

695 **Fig. 1S.** The heterogeneous reaction of OCS on 50.2 mg of α-Al_2O_3 at 300 K (left side)

696 and the *in situ* desorption of surface species in the end of uptake (right side).

697

698

699

700

701

702

703

704

705

706

707

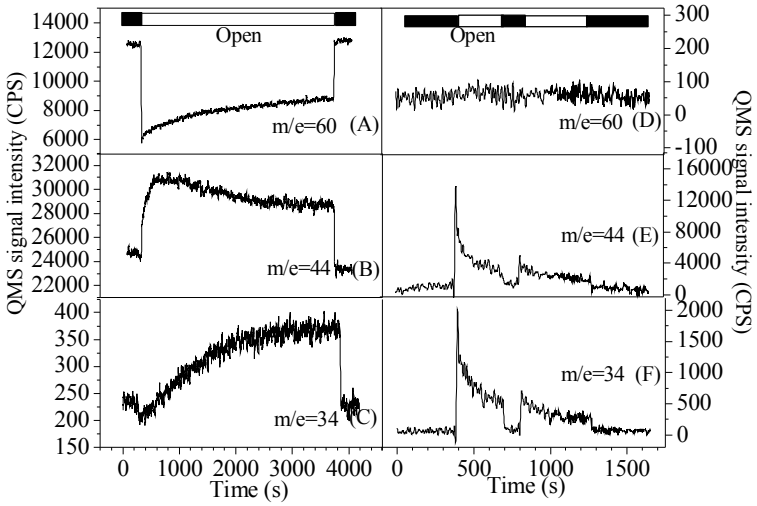

Fig. 2S. The heterogeneous reaction of OCS on 100.0 mg of MgO at 300 K (left side) and the *in situ* desorption of surface species in the end of uptake (right side).

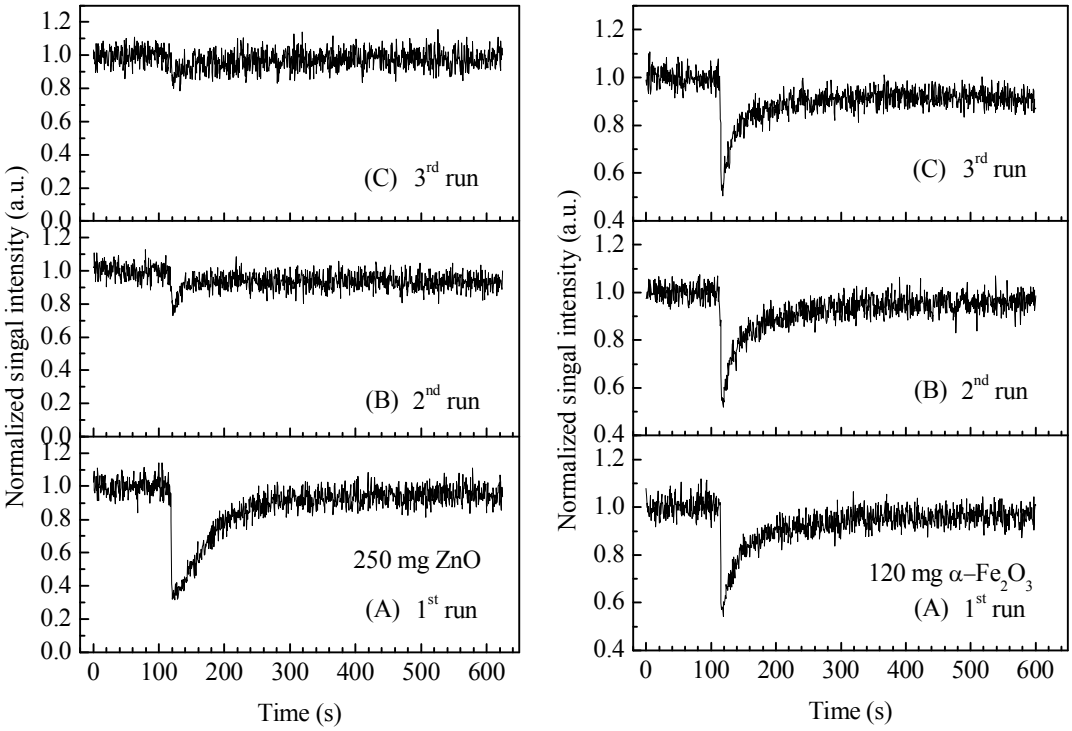

Fig. 3S. Repeated uptake experiments of OCS on ZnO and α-Fe_2O_3. Uptake experiments were performed at 300 K. After the uptake experiment finished, the sample were out-gassed at $3.0\pm1.0\times10^{-7}$ Torr and at 300 K for 18 h.